ELSEVIER

Journal of Alloys and Compounds 452 (2008) 425–431

Journal of ALLOYS AND COMPOUNDS

www.elsevier.com/locate/jallcom

Study on low-cycle fatigue behaviours of the aluminium cast alloys

D. Ovono Ovono [a,*], I. Guillot [b], D. Massinon [c]

[a] *University of Technology of Compiègne, Laboratoire Roberval, 60205 Compiègne, France*
[b] *Centre d'Etudes de Chimie Métallurgique, UPR CNRS 2801, 15 rue Georges Urbain, 94407 Vitry-sur-Seine, France*
[c] *Fonderie Montupet, 67 rue J. de la Fontaine, 60181 Nogent-sur-Oise, France*

Received 16 February 2006; received in revised form 31 October 2006; accepted 14 November 2006
Available online 5 December 2006

Abstract

The effect of aging, Si, Fe and Mn content on the fatigue behavior of two cast aluminium A319 and AS9U3G alloys, in the T5 state, were investigated. The low-cycle fatigue (LCF) was conducted on these alloys and results were analyzed with respect to the evolution of the microstructure and the fatigue fractured surface examination. In the alloy with a high content of Si, Fe and Mn (AS9U3G) the fatigue life is significantly reduces. The high decrease in normalized amplitude and back stresses at the saturation state, just after 200 °C, has been interpreted, in the A319 alloy, as a transition between θ′ in Si, Q and θ precipitates and AS9U3G alloy presents the same transition. Therefore, the increase in Si content and/or residual elements contents does not alter the precipitation mechanism. Aging (100 h at 320 °C) of both alloys has resulted in an increase in fatigue life and secondary cyclic hardening which corresponds to an increase in back stress due to the heterogeneous structure of dislocation formation. The calculation of back stress is in good agreement with the experimental results.

Keywords: T5 treatment; Intermetallic compounds; Precipitation; Low-cycle fatigue

1. Introduction

In recent production, Al–Si–Cu cast alloys have been used so far because of their good performance of castability and mechanical strength with age hardening. Age hardening affects not only the mechanical strength but also the thermal fatigue properties. The strengthening of these alloys is usually realized through precipitation hardening. A lot of effort has been spent on investigation of the precipitation process in Al–Si–Cu alloys. It is well known that the subsequent evolution of the microstructure corresponds to the decomposition of the solid solution oversaturated in GP zones, the θ″ phase, the θ′ phase, and the stable phase θ. For the development of a new cylinder head and in order to lower the costs of provision at the refiner, we have chosen to increase the iron, manganese, and zinc contents used in A319 alloys. These residual elements were increased the formation of intermetallics compounds. The low-cycle fatigue (LCF) tests were carried out on different alloys in order to study their mechanical behaviour. Studies of the behaviour of a material under LCF conditions are important from the point of view of cracking and failure of material. The fatigue behaviour of these alloys and their properties depends on the nature, the size, and the hardening phases distribution [1]. The effects of porosity [2,3] and intermetallics [4–6] are well established. Dislocations cut the precipitates of small size and/or coherent with the matrix whereas large and/or incoherent precipitates are looped by dislocations. This interaction mechanism between the dislocations and precipitates are important with regards to the view properties of the material. Studies done on the foundry Al–Si–Cu alloys have indicated that the fatigue life of these alloys is influenced by shrinkage cavities, size of the dendrite, size and morphology of silicon and intermetallic compounds. Fatigue cracks in these cast alloys often initiated in interdendritic casting defect [7], to the surface close to the porosities [8], and by the eutectics particles [9].

In the present study, we investigated the microstructure of cast aluminium alloys by scanning electron microscopy–energy dispersive spectrometry (SEM–EDS), transmission electron microscopy (TEM) analysis. TEM analysis was used to obtain information on the mechanisms and kinetics of particle growth and the impact of residual element, temperature and aging on the low-cycle fatigue properties was examined. Current model was used to calculate the back stress.

* Corresponding author. Tel.: +33 3 44 23 44 23; fax: +33 3 44 23 44 15.
E-mail address: delavand.ovono-ovono@utc.fr (D. Ovono Ovono).

0925-8388/$ – see front matter © 2006 Elsevier B.V. All rights reserved.
doi:10.1016/j.jallcom.2006.11.052

Table 1
Chemical compositions (wt%) of the two kinds of aluminium alloys

	Si	Cu	Mg	Fe	Mn	Al
A319	7	3	0.3	0.1	0.1	Rest.
AS9U3G	9	3	0.3	0.7	0.5	Rest.

2. Experimental

2.1. Materials

An industrial A319 alloy and AS9U3G alloy with a high content of Fe, Mn and Zn were used for this study. The eutectic Si particles were modified by using 250 ppm of Sr and Na and a commercial Ti-B grain refiner was also added. The chemical compositions of different alloys in this work are given in Table 1. The specimens were heat-treated to the T5 condition, i.e. solution treated at 490 °C in an air furnace, water quenched at room temperature, naturally aged at room temperature, and then artificially aged at 210 °C for 5 h. In this treatment, alloys reached the peak hardness. In addition to the T5 heat treatment, other aging treatments (100, 200, 250, 280 and 320 °C for 100 h) were also utilized, to evaluate the influence of aging on the microstructure and on the low-cycle fatigue.

2.2. Procedure

After T5 treatment, and the aged samples blocks were machined into cylindrical fatigue specimens, with 15 mm gauge length and with 8 mm diameter. The alloys were subjected to a low-cycle fatigue test under a plastic strain control ($\Delta\varepsilon_P/2 = 0.3\%$) at different temperatures on a servohydraulic machine. Each test was performed at constant strain rate $6 \times 10^{-4}\ s^{-1}$, and the axial strain was determined using an extensometer with its arm tips located on gage length. All these mechanical tests were carried out until the material failed. The samples were tested at different temperature for T5 specimens, and at room temperature for aged specimens. The tensile flow stress of fatigue tests was divided into two components: an effective stress, Σ_{ef}, and a back stress, X, according to the feature of hysteresis loops obtained by unloading tests. The analysis proposed by Dickson et al. [10] and Feaugas [11] was used to provide a stress partition, taking into account the thermal part of the flow stress, Σ^* (Fig. 1):

$$\Sigma_{ef} = \frac{1}{2}(\Sigma - \Sigma_r) + \frac{\Sigma^*}{2} \quad (1)$$

$$X = \Sigma - \Sigma_{ef} \quad (2)$$

where the reverse yield stress, Σ_r, is obtained with a plastic strain offset equal to $3 \pm 2 \times 10^{-5}$.

The back stress, which is directional component of hardening, is linked to the local straining process that introduced long-range interaction with mobile dislocations. The effective stress component is an isotropic component. This stress component represents the stress locally required for a dislocation to move (short-range interactions). In stress space, the effective and back stress correspond, respectively, to the radius and the shift of yield surface.

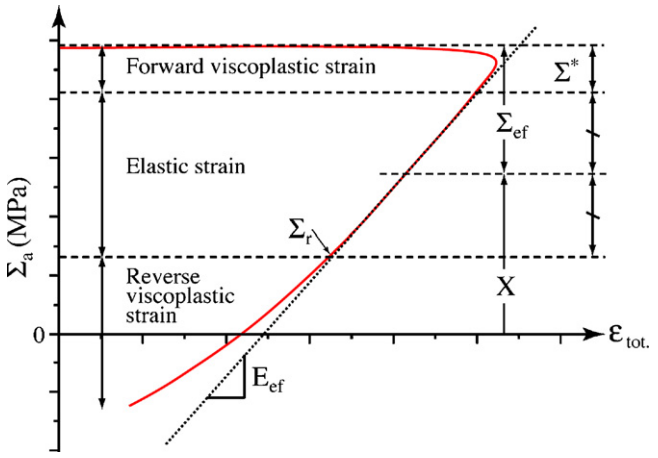

Fig. 1. Flow stress partition in term of back, X, and effective, Σ_{ef}, in an hysteresis loop [11]. Σ_r is the stress where reverse plastic strain occurs, and Σ^* is the thermal part of the effective stress.

Standard optical metallography, scanning electron microscopy, transmission electron microscopy (STEM) were carried out on selected samples for different experimental conditions. Energy dispersive spectroscopy was utilised to identify the different type of phases present on the alloys. To investigate the fracture mode and fatigue crack initiation sites, fractured surfaces were examined after the LCF test using a SEM.

3. Results

3.1. Microstructural observations

The average secondary dendrite arm spacing (SDAS is the distance between centers of the adjacent dendrite arms of the microstructure) was 20 μm (low SDAS). The microstructure of T5 material (Fig. 2) consists of a dendritic aluminium α-phase containing Cu and an aluminium–silicon eutectic with intermetallics compounds between dendritic arms. The EDS analysis revealed that the compounds formed in the both alloys during solidification are "Chinese script" α-$Al_{15}(Fe,Mn)_3Si_2$ intermetallic phases (Fig. 3a), plate shaped β-Al_5FeSi phase particles, Al_2Cu phases (Fig. 3b) and Q-$Al_5Cu_2Mg_8Si_6$.

Fig. 4 shows bright-field TEM images of the alloys at the T5 condition. The aging treatment occurs in two steps: T5 aging, where θ′ precipitates were present, aging at 200 °C for 100 h, where θ′ precipitates obtain their optimal size and are then gradually replaced by the Si, θ and Q precipitates. After an aging superior to 200 °C, the microstructures of the both

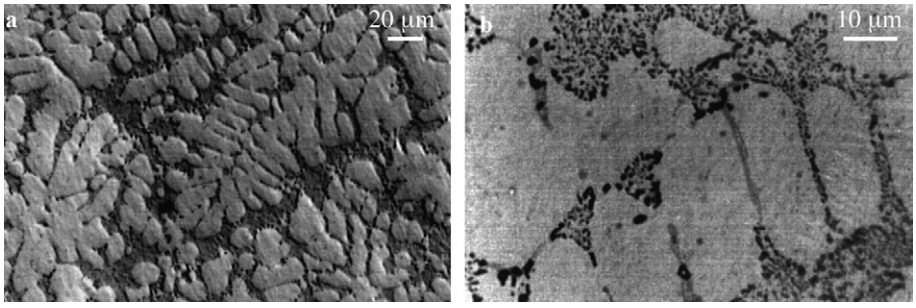

Fig. 2. Optical micrographs of the T5 A319 showing (a) dendrites (b) interdendritic space.

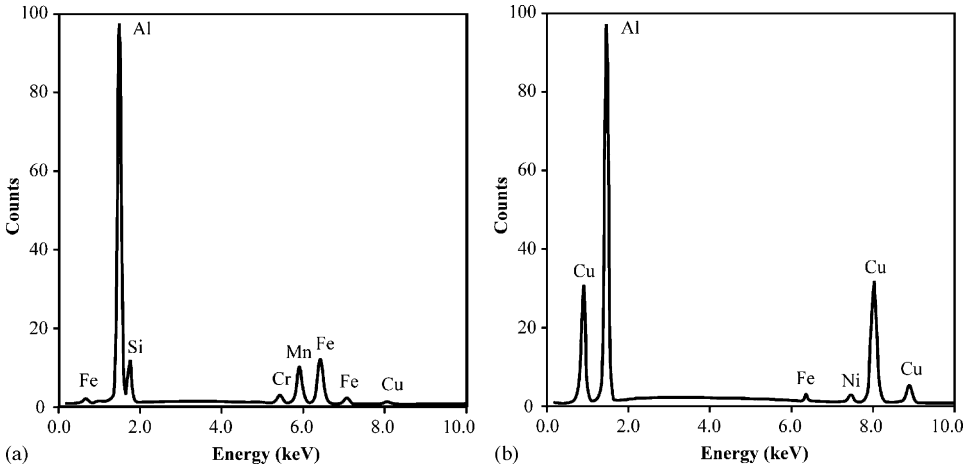

Fig. 3. EDS spectrum of particles in the inter dendritic space (a) α-$Al_{15}(Fe,Mn)_3Si_2$ intermetallics and (b) Al_2Cu phase.

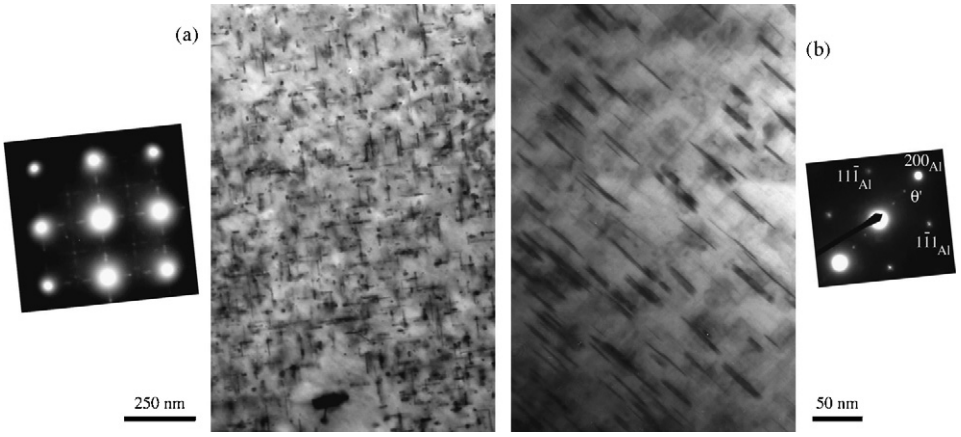

Fig. 4. Bright-field TEM micrographs ($[0\,0\,1]_{Al}$ zone axis) after T5 treatment needle-like θ′ precipitates and selected area diffraction patterns (a) A319 alloy and (b) AS9U3G alloy.

alloys (Fig. 5) present the Q laths appear in the $[0\,0\,1]_{Al}$ orientation, θ phase and Si phase which are incoherent with the matrix lattice. It is clear that the precipitation sequence in the both alloys as the aging temperatures increases is essentially: $\theta' \rightarrow Q + Si + \theta$ (Al_2Cu). The Table 2 presents the precipitation evolution after some treatment. The information available on equilibrium in Al–Si–Cu–Mg alloys suggests, depending on the alloy composition, one or more of the phases Si, Al_2Cu-θ and Q-$Al_5Cu_2Mg_8Si_6$ may appear as dispersoids [12]. Lloyd [13] has observed large dispersoids containing Fe, Mn, Si and Al in Al–Si–Cu–Mg alloys containing Mn, Fe. The work of Takeda et al. [14] shows that Mn additions, in a Al–Cu alloy, stabilize the structure of the θ′ phase. Due to the stabilization effect, the coarsening of the intermediate θ′ phase is reduced in the aging process of an Al–Cu–Mn alloy. Apparently, in the present work, increasing the concentration of Si, Fe, Mn do not alter the precipitation mechanism. Increasing the concentration of Si, Fe and Mn, in AS9U3G, resulted in a visible increase in the amount of intermetallics.

3.2. Effect of temperature on LCF behaviour

The stress response with respect to the number of cycles is an important characteristic of fatigue process. The curves of cyclic hardening provide some information on the mechanical stability of the material. Fig. 6 shows the variation of the stress amplitude, Σ_a, with the cumulated plastic strain controlled ($\Delta\varepsilon_P/2 = 0.3\%$). Cyclic stabilisation behaviour is evident throughout all temperatures and is proceeded by detectable cyclic hardening only at lowest temperature ($T < 250\,^{\circ}C$). These curves show influence of temperature on these alloys due to the microstructural evolution. At low temperature the stress ampli-

Table 2
Evolution of precipitation after some treatment

	100 h at 100 °C	100 h at 200 °C	100 h at 250 °C	100 h at 280 °C	100 h at 320 °C
A319 (T5)	θ′	θ′	θ, Q, Si	θ, Q, Si	θ, Q, Si
AS9U3G (T5)	θ′	θ′	θ, Q, Si	θ, Q, Si	θ, Q, Si

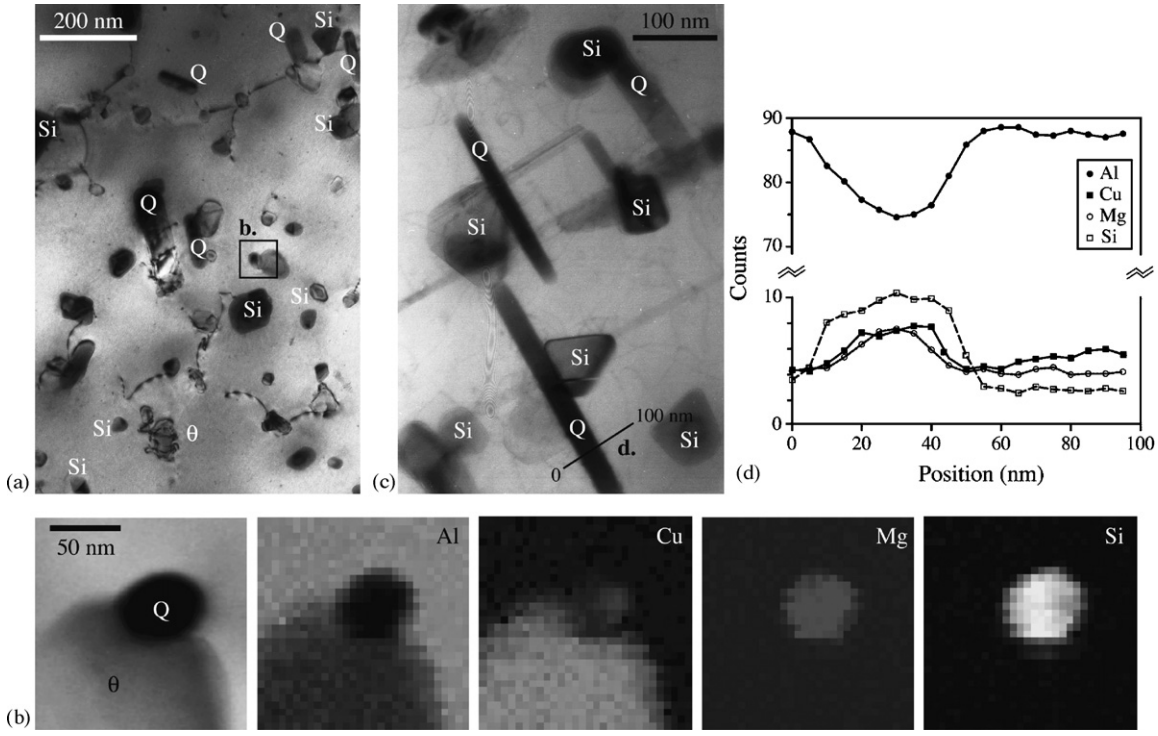

Fig. 5. TEM micrographs aging 100 h at 320 °C after T5 treatment (a) A319 alloy and (c) AS9U3G alloy. (b) Element mapping of Q-$Al_5Cu_2Mg_8Si_6$ precipitate and (d) EDS spectrum of Q precipitate.

tude of AS9U3G alloy is slightly higher than A319. The A319 alloy for all temperature has significantly greater fatigue life compared to AS9U3G alloy, this can especially be seen in Fig. 6. Both temperatures 20 and 100 °C for those samples have similar fatigue strength. After 100 °C, increasing the temperature results in decrease in the fatigue strength. It can be seen that an increase in temperature led to an increase in the size of θ′ precipitates [15]. It can also be seen that the density of θ′ precipitates decreases with the temperature [16]. This decrease could have contributed to the decrease in stress amplitude. It is well known that the strengthening mechanism on these kinds of alloys is essentially due to the dislocation interaction with the precipitates. A study carried out by Calabresse and Laird [17] on a binary alloy AU4 in presence of θ′ precipitates showed this type of behaviour with cyclic hardening. Therefore, the dislocations are going to assemble around θ′ semi-coherent precipitates and causing a hardening in the material. This regrouping of the dislocations is at the origin of a stress field around θ′ precipitates resulting in local stress in the material. Therefore, the strengthening mechanism observed is due to the dislocation interaction with the precipitates.

3.3. Effect of aging on mechanical behaviour

The evolution of the stress amplitude versus cumulated plastic strain (Fig. 7) clearly shows the effect of aging on mechanical properties. Aging affects the stress amplitude and the fatigue life of these materials. The density of obstacles and the nature of the dislocation–obstacle interactions vary during aging. The high test temperature and aging involve to a reduction of yield strength and ultimate tensile stress due to an increasing of the

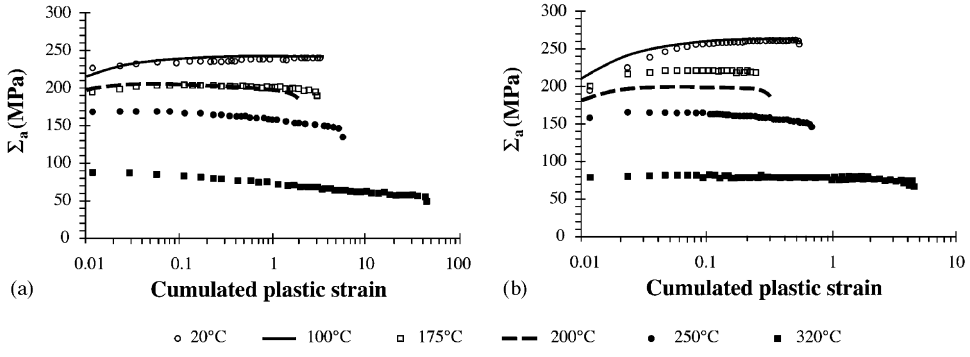

Fig. 6. Stress amplitude evolution during low-cycle fatigue test with imposed plastic strain amplitude ($\Delta\varepsilon_P/2 = 0.3\%$) of the both alloys after T5 treatment (a) A319 alloy and (b) AS9U3G alloy.

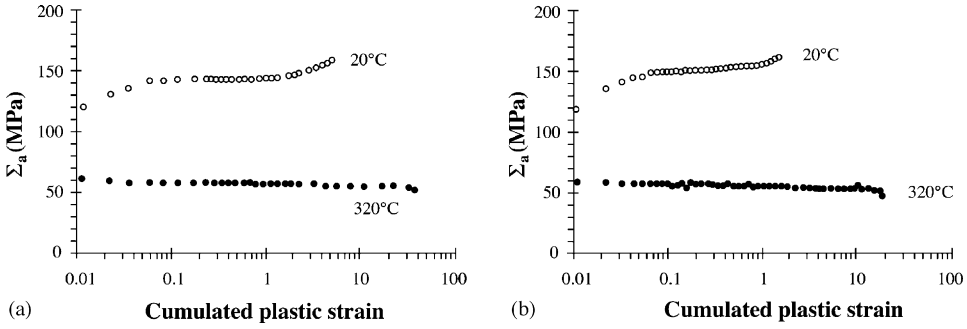

Fig. 7. Stress amplitude evolution during low-cycle fatigue test with imposed plastic strain amplitude ($\Delta\varepsilon_P/2 = 0.3\%$) of the both alloys heated 100 h at 320 °C after T5 treatment (a) A319 alloy and (b) AS9U3G alloy.

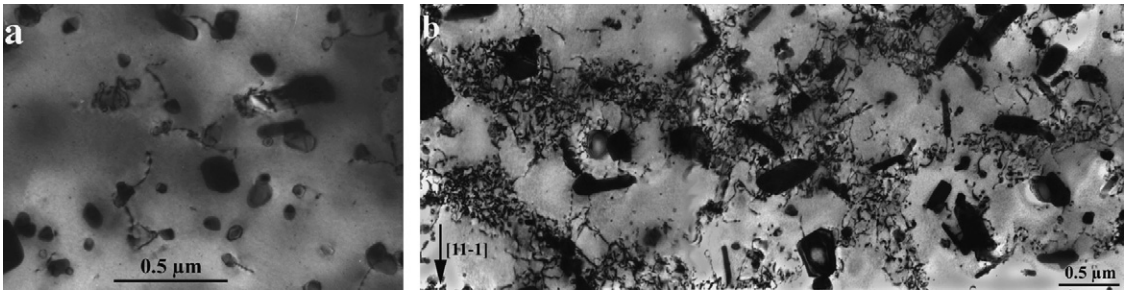

Fig. 8. STEM micrographs of A319 alloy (a) without secondary cyclic hardning and (b) with secondary cyclic hardning. Comparison of both figures suggests that secondary cyclic hardning is due to the heterogeneous structure of dislocations leaning on the precipitation.

distance between particles. Besides, it can be observed that the aging improves considerably the fatigue life of these alloys as a result of the evolution of the precipitation due to the aging treatment. The fatigue life is enhanced after aging (see Table 2), which may be due to the precipitation transformation. It can be also seen that, at 20 °C, the alloys aging during 100 h at 320 °C display secondary hardening. To explain this behaviour, TEM observations at this stage of secondary hardening were carried. These observations show that (Fig. 8) this secondary hardening corresponds to an increase in back stress due to the setting up of heterogeneous structure of dislocations leaning on the precipitation. The present results clearly show an effect of residual elements content on low-cycle behaviour, mainly the loss of fatigue life.

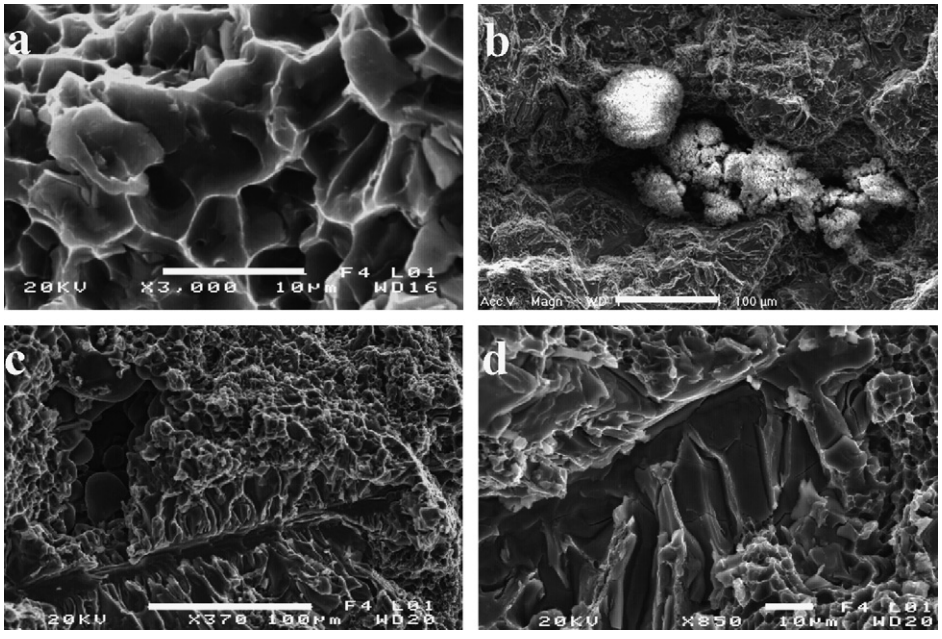

Fig. 9. SEM fracture morphology showing (a) ductile fracture; (b) oxide film; (c) porosity near intermetallic compounds; and (d) intermetallic compound.

3.4. Fracture surface observations

The mechanical properties of these alloys can deteriorate due to the presence of pores, oxide films, intermetallic compounds, and the other defects. The introduction of a large content of residual elements increases the density, the size of intermetallic compounds and the porosities. It was determined that in the both alloys, α-$Al_{15}(Fe,Mn)_3Si_2$ particles form in addition to the dispersion of β-Al_5FeSi. These particles tend to be large and brittle and are known to lower the fatigue life alloy. It seems reasonable to expect the same deleterious effect on the present alloys. The SEM fractographs of the LCF tests are approximately the same for the two alloys. All the fracture surfaces show a mixed mode of ductile fracture and brittle fracture. The fatigue cracks initiated primarily at large pores, intermetallics, located close to, or at, the specimen surface (Fig. 9), after the fatigue cracks quickly propagate and coalesce with the other defects. The main difference between alloys A319/AS9U3G is that the latter contains more intermetallics compounds and porosities than the first. Therefore, the reduction of the fatigue life in AS9U3G alloy is essentially due to an increasing in residual elements content.

4. Discussion

4.1. Stresses partition

Fig. 10 presents the partitions of stresses to the level of the landing of saturation returned to the shear modulus, μ, according to the test temperature. The partition of the macroscopic stress, in back stress, and in effective stress showed that the evolutions of the macroscopic and back stresses are similar. This indicates that the evolution of the macroscopic stress is directly related to the evolution of the back stress X. High reduction in stress Σ_a just after 200 °C is observed. This high decrease in stress Σ_a can be directly associated with the precipitation transformation due to the test temperature. In the A319 alloy, it has been observed [15] that after aging of 100 h at 100 °C the density of θ′ precipitates decreases and the increase in aging temperature leads to an increase in the size of these precipitates. After aging of 100 h at 200 °C the transition of θ′ to Q, θ and Si precipitates have been observed. From the results shown, it is possible to suggest that the reason for the decrease in stress amplitude and in back stress is due to the transformation of θ′ to Q, θ and Si precipitates. The same high reduction of Σ_a is observed in AS9U3G alloy. This study also shows that the behaviour of the material in fatigue is therefore, largely governed by back stress to long distance due to heterogeneity and to the evolution of the microstructure.

4.2. Back stress modelling

To calculate the stresses in the particles we need to consider the different sources of stress. Taking account of different particles present on the inter dendritic space, in plastically deformed regions, the back stress developed on the eutectic particles can be calculated as presented:

- At low strains [18]:

$$X_1 = 2.14\alpha_0\mu f\varepsilon^* \tag{3}$$

- Similarly, at large strains [19]:

$$X_2 = C(1 + f^{1/2})\mu\sqrt{b\left(\frac{C_1}{L} + \frac{C_2}{D}\right)(\varepsilon - \varepsilon_C^*)} \tag{4}$$

where μ is the shear modulus of Al matrix, α the aspect ratio of particles, f the volume fraction of particles in the inter dendritic space, ε^* the unrelaxed plastic strain, ε the tensile strain, ε_C^* the plastic strain at the onset of plastic relaxation, L the average slip distance, λ the dendritic grain size (SDAS = 20 μm), b the Burgers vector and C, C_1 and C_2 are constants. For cast aluminium alloys, Brown [20] gives the following values for the constants: $C \approx 1.25$, $C_1/L \approx 0.05\ \mu m^{-1}$ and $C_2 \approx 2$.

Thus, assuming simple addition of these two components X_1 and X_2, the back stress at the saturation, X, in function of the aging temperature is given by:

$$X = X_1 + X_2 \tag{5}$$

Fig. 11 shows the results of measured and calculated values of back stress. It is seen that the agreement between measured and calculated values is very good. Thus, this study shows that the analysis proposed by Dickson et al. is good to determine the back stress.

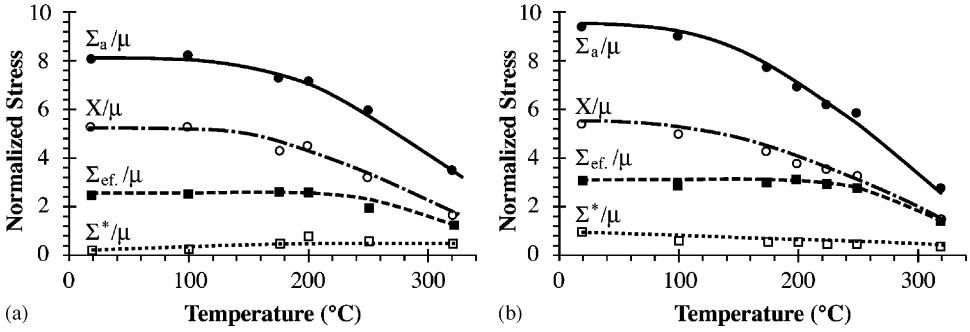

Fig. 10. Evolution of normalized stresses (Σ_a: stress amplitude, X: back stress, Σ_{ef} effective stress, Σ^*: the thermal part of the effective stress, μ: the module of shearing) according to the test temperature (a) A319 and (b) AS9U3G.

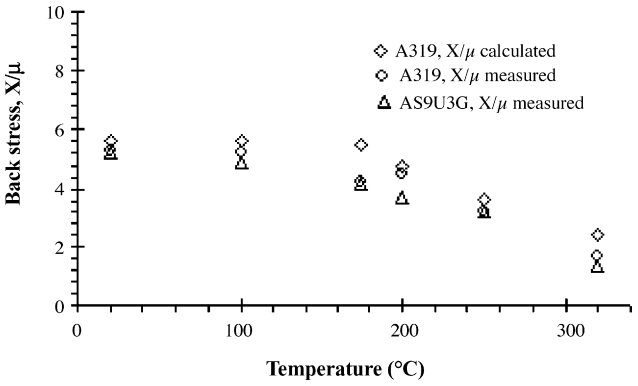

Fig. 11. Comparison of the experimental and modelling results of back stress.

5. Conclusions

(1) The microstructure results show that the nature of compounds formed on these alloys are not influenced by the increase in residual elements content, but only the number of these compounds is influenced.
(2) By increasing the residual elements content, the density, the size of intermetallics compounds, and the volume of defects were considerably increased. AS9U3G alloy presents many large pores and intermetallic compounds which are fatigue crack initiated. The fatigue life of the AS9U3G alloy is much smaller than that of A319. Therefore, the fatigue life of these alloys is essentially controlled by the density of intermetallics compounds and the volume fraction of pores.
(3) The partition of the macroscopic stress shows that the evolution of the macroscopic stress is directly related to evolution of the back stress X due to the heterogeneity and the evolution of the microstructure. The calculated back stress, with a current model, is consistent with obtained values by the Dickson et al. analysis.

Acknowledgements

The authors would like to thank the Région Picardie for its financial support. They are grateful to T. Voitot, G. Marichal, J.P. Wtyklo and R. Leblond for useful technical assistance.

References

[1] M.J. Caton, J.W. Jones, J.A. Allison, Metall. Mater. Trans. 30A (12) (1999) 3055.
[2] A.M. Samuel, F.H. Samuel, Metall. Mater. Trans. 26A (2) (1995) 2359.
[3] N. Roy, A.M. Samuel, F.H. Samuel, Metall. Mater. Trans. 27A (2) (1996) 415.
[4] G. Gustafsson, T. Thorvaldsson, G.L. Dunlop, Metall. Trans. 17A (1) (1986) 45.
[5] A.M. Samuel, J. Gautier, F.H. Samuel, Metall Mater. Trans. 27A (1996) 1785.
[6] S. Hirosawa, T. Sato, A. Kamio, H.M. Flower, Acta Mater. 48 (2000) 1797.
[7] Q.G. Wang, D. Apelian, D.A. Lados, J. Light Metals 1 (2001) 73.
[8] J.C. Ting, F.V. Lawrence, Fatigue Fract. Eng. Mater. Struct. 16 (1993) 631.
[9] Q.G. Wang, D. Apelian, D.A. Lados, J. Light Metals 1 (2001) 85.
[10] J.L. Dickson, L. Handfield, G. L'Esperance, Mater. Sci. Eng. 60 (1983) 3.
[11] X. Feaugas, Acta Mater. 47 (13) (1999) 3617–3632.
[12] D.L.W. Collins, J. Inst. Met. 86 (1957–1958) 325–336.
[13] D.J. Lloyd, 'Microstructural development in AA 2038 alloy' report no. KR-82/030, Alcan International Ltd, Kingston, 1982.
[14] M. Takeda, A. Komatsu, M. Ohta, T. Shirai, T. Endo, Scripta Mater. 39 (9) (1998) 1295–1300.
[15] D. Ovono Ovono, I. Guillot, D. Massinon, Scripta Mater. 55 (2006) 259–262.
[16] B. Barlas, D. Ovono Ovono, I. Guillot, G. Cailleteau, Mater. Sci. Forum 396–402 (2002) 1365–1370.
[17] G. Calabresse, C. Laird, Mater. Sci. Eng. 13 (1974) 141.
[18] Q.G. Wang, D. Apelian, D.A. Lados, J. Light Metals 1 (2001) 85–97.
[19] C.H. Cáceres, J.R. Griffiths, P. Reiner, Acta Mater. 44 (1) (1996) 15–23.
[20] L.M. Brown, Acta Metall. 21 (1973) 879–885.